Proportional-Integral Passivity-based Control of a Fuel Cell System with an Energy Storage System

Carlo A. Beltrán, Diego Langarica-Cordoba, Luis H. Diaz-Saldierna, Rafael Cisneros, Panfilo R. Martinez-Rodriguez

***Abstract*—This paper presents a proportional-integral passivity-based control (PI-PBC) approach for a system consisting of a proton-exchange membrane fuel cell as the primary energy source and a super-capacitor as an auxiliary energy storage device. Its objectives are to regulate the output and super-capacitor voltages while smoothing variations in the energy extracted from the cell. The controller design leverages the difference in time-scales , enabling the system dynamics to be partitioned into fast currents and slow voltages. It follows a current-mode control framework, where both inner and outer loops are developed using the PI-PBC methodology. The inner loop adjusts the duty cycles to track current reference trajectories, while the outer loop generates these references to regulate voltages. Additionally, an adaptive law based on Immersion and Invariance theory enhances the robustness of the outer loop controller. Numerical simulations validate the proposed approach, demonstrating stability and precise regulation despite pulsating energy demand.**

***Keywords*—Energy Storage Systems, Online Estimation, Passivity-based Control, Polarization Curve, Proton Exchange Membrane Fuel Cell, Supercapacitor**

I. Introduction

Clean energy applications of significant interest encompass microgrids, transportation electrification, and energy storage systems (ESSs), where one of the primary objectives is the reduction of greenhouse gas emissions. Among the various clean sources, fuel cells are considered next-generation devices. This is attributed to advantages such as high energy density, non-intermittent operation, high efficiency, and the use of hydrogen-rich fuels, among others [1]. A type of fuel cell that stands out for its high efficiency, low operating temperature, and scalability is the proton-exchange membrane fuel cell (PEMFC). A single fuel cell generates a small amount of energy, so to meet higher power demands, cells are grouped in series-parallel arrays. This configuration enables fuel cells to supply energy for a wide range of applications, from low to high power. For example, for the electric bus of 150 kW "UC Irvine AFCB". And larger arrays can be made for applications such as stationary power systems and microgrids [2]. Nevertheless, this technology faces numerous challenges for its proper implementation. Some of these challenges include their short lifespan, which can be further reduced by very steep energy variations, slow dynamic response, as well as the highly nonlinear relationship between the voltage-current supplied [3]. Additionally, obtaining the cell model is a difficult task due to its complex dynamics, arising from the interaction of multiple phenomena.

The use of power converters as an interface is a well-documented method for regulating the output voltage of an energy source to the desired level. Integrating a power converter between the cell and the load results in a fuel cell system capable of delivering regulated power. Adding more energy sources into the DC bus can enhance system performance and reduce fuel consumption. For instance, with its high power density, the super-capacitor (SC) can rapidly supply or store energy to meet high-power demands, enabling regenerative braking. A battery provides high energy storage capacity, while an electrolyzer enables to store energy in the form of hydrogen, among other possibilities. Regenerative braking is crucial for transport electrification, electrolyzers support energy storage systems, and the DC bus voltage can be utilized in DC microgrids. However, as the complexity of the system increases, so does the difficulty of the controller design. For example, in [4], a control system is developed for a fuel cell system with a battery, which is connected to the DC bus via a bidirectional converter. Its objective is DC bus regulation, achieved indirectly. The control signals are computed using traditional passivity-based control (PBC), formulated with the Euler-Lagrange approach and employing the energy shaping and damping injection methodology. A power management strategy distributes the demand between both sources, with the battery serving as a support. This controller is improved by making it adaptive in [5], where the load, an uncertain and time-varying parameter, is estimated online with an integral action. On the other hand, in [6], an adaptive controller is developed for a slightly modified system, where a SC replaces the battery. Its objectives are to regulate the output and SC voltages while smoothing variations in the energy extracted from the cell. Its methodology is based on singular perturbation theory and employs current-mode control. The control structure consists of an inner loop that tracks the reference current trajectories and an outer loop that generates current references for voltage regulation. The inner loop is designed using a classical PI controller, while the outer loop employs a backstepping approach. Additionally, load estimation is incorporated to enhance the robustness of the outer loop. In [7], a control strategy is developed for a system similar to the previous one, aiming to indirectly regulate the output voltage. The control signals are computed using PBC with interconnection and damping assignment. This

Carlo A. Beltrán, Diego Langarica-Cordoba, Luis H. Diaz-Saldierna, Panfilo R. Martinez-Rodriguez are with the School of Sciences, Autonomous University of San Luis Potosi (UASLP), Av. Chapultepec 1570, Priv. del Pedregal, 78295, San Luis Potosi, Mexico. (e-mail of corresponding author: diego.langarica@uaslp.mx). R. Cisneros is with the Department of Electrical and Electronic Engineering, Instituto Tecnologico Autonomo de Mexico, Río Hondo 1, Ciudad de Mexico 01080, Ciudad de Mexico, Mexico (e-mail: rcisneros@itam.mx).

Paper submitted to the International Conference on Power Systems Transients (IPST2025) in Guadalajara, Mexico, June 8-12, 2025.

approach employs the Hamiltonian representation and aims to impose a desired closed-loop dynamic behavior through the design of the control signal. The cell current reference is generated by an outer PI loop, while the SC reference is determined based on its equilibria. In [8], the same PBC strategy is applied to a similar system, replacing the SC with a battery. The objective remains the regulation of the DC bus, where the battery is considered a support source. Unlike previous approaches, current references are generated based on an energy management strategy. A drawback of the aforementioned controllers is their reliance on load knowledge. Moreover, these models do not consider parasitic resistances, which play a crucial role in accurately representing real-world conditions. Reference [9] presents a control strategy for an isolated DC microgrid comprising a battery, PEMFC, and electrolyzer interconnected via bidirectional converters. The microgrid connects to a DC bus that integrates renewable sources such as wind and solar. Using the same PBC strategy as before, the system regulates the output voltage by storing excess energy as hydrogen for later conversion. Integral action compensates for parasitic resistances, while sliding mode control limits bus voltage fluctuations. Like previous controllers, it requires knowledge of the load.

For a fuel cell system with a SC, the following are the main contributions of this research regarding to the output voltage and SC regulation, while smoothing variations in the energy extracted from the cell:

- The proposed control scheme follows a current-mode control approach, implementing a simple and easy-to-tune two-loop PI-PBC structure.
- To ensure stability, the design exploits the monotonic behavior of the fuel cell polarization curve.
- To enhance robustness, an adaptive law based on Immersion and Invariance (I&I) theory is incorporated into the outer loop controller.
- Unlike previous studies, this approach explicitly accounts for system parasitic resistances by integrating them into a voltage drop model. Moreover, it does not require prior knowledge of the load, an uncertain and time-varying parameter and is computationally less demanding than some previously proposed methods.

Notation. I_n is the $n \times n$ identity matrix. A column vector is denoted $a = \text{col}(a_1, a_2, \ldots, a_n) \in \mathbb{R}^n$. $\mathcal{L}_2$ is referred as the set of square-integrable functions $f : \mathbb{R}_+ \to \mathbb{R}$, namely, they satisfy $\int_0^\infty |f(t)|^2 dt < \infty$.

II. System description

Fig. 1 illustrates that the system under study comprises two energy sources, a PEMFC for generation and a SC for storage. In order to supply regulated energy, a protection diode and a boost converter are used as interfaces between the load and the cell. Furthermore, a bidirectional buck-boost converter is used as the interface between the SC and the load. Thus, the cell voltage can be raised to the desired operation level, while the SC can either supply energy in a boost mode or recover energy in a buck mode, depending on the control system requirements. In this topology, the SC plays a major part in the energy supply by managing fast transients. This allows the energy extracted from the PEMFC to vary smoothly until it completely meets the demand. It is emphasized that rapid variations in energy reduce the cell lifespan [3]. The system comprises the following elements: two energy sources, the PEMFC which is protected from reverse flow by a protection diode D_p and a SC whose leakage resistance R_{p3} is considered, two inductors L_1 and L_2 and their respective parasitic resistance R_{p1} and R_{p2}, three MOSFET switching devices M_1, M_2, and M_3, the boost converter diode D, a DC link capacitor C, and a purely resistive load R_L. The system signals are the currents i_{fc} and i_{sc} that are respectively the cell current and the SC current, the voltages v_{fc}, v_{sc}, and v_o, that are respectively the cell voltage, the SC voltage, and the output voltage, and the PWM signals q_1, q_2, and q_3 that drive its respective MOSFET.

The PEMFC dynamics result from the interaction of multiple phenomena and systems, making its modeling a complex task. This system converts hydrogen and oxygen into electrical energy, heat, and water through an electrochemical reaction. This process relies on the interaction of multiple systems such as humidification, temperature regulation, and precise control of the oxygen and hydrogen supply, among others. Capturing this complex dynamics results in high-order models, which makes them computationally demanding. Hence, for power system applications, the cell is usually modeled statically using its polarization curve. A highly non-linear relationship between the voltage and current it supplies. In this work, the power function model, detailed in [10], is used to describe this relationship as:

$$v_{fc} := V_{fc}(i_{fc}) = E_{oc} - a_1 i_{fc}^{a_2}, \tag{1}$$

where E_{oc}, the voltage measured in no-load operation, is the open-circuit voltage, and the parameters a_1 and a_2 are positive, constant, and unit-less values. Both the parameters a_1 and a_2 are computed offline from average experimental data fitting procedures and E_{oc} through a measurement. This model accurately describes the polarization curve behavior of the cell, it captures the three voltage drops named activation, ohmic, and concentration. Furthermore, this model has been employed to experimentally validate control strategies for regulation purposes [11]. To simplify the overall system model, the SC is

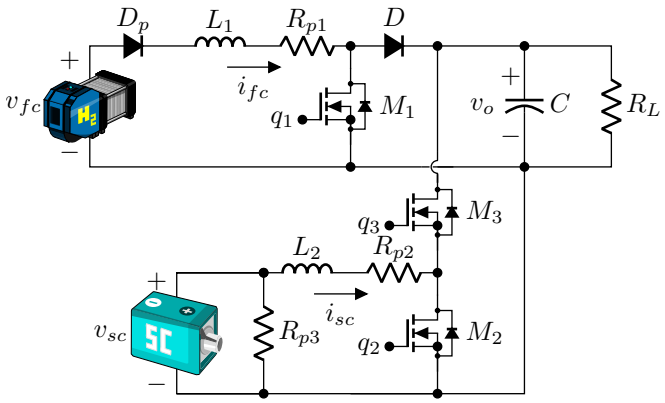

Fig. 1: Fuel cell system (FCS) with a SC-based ESS under consideration.

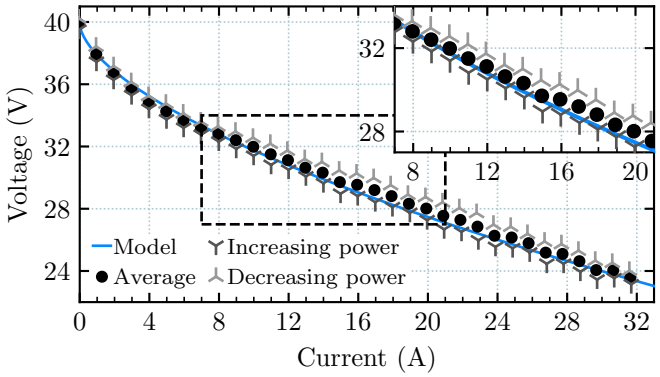

Fig. 2: Model of the 1.2 kW PEMFC Nexa® automatic power module polarization curve, characterized by parameters $E_{oc} =$ 38.8697 V, $a_1 =$ 1.995, and $a_2 =$0.6100.

represented with an electric equivalent circuit model, as detailed in [12, Fig. 4(a)]. This model includes a capacitor to represent its capacitance, an equivalent series resistor to account for internal resistance, and an equivalent parallel resistor R_{p3} to model the leakage current. The leakage resistance is included to support the stability analysis, while the series resistance is merged with the parasitic resistance of the inductor R_{p2}.

Experimental current-voltage measurements obtained from the 1.2 kW PEMFC Nexa® power module are used for validation purposes. These measurements can be observed in Fig. 2, where the complex hysteresis phenomena appears as the power is increased and subsequently decreased. Then, *offline*, average values are computed and used in data fitting procedures to obtain the model parameters a_1 and a_2. The *monotonicity property of the polarization curve*, described in [13, Lemma 1], is also used in this work to support the stability analysis. Thus, for completeness, it is described below.

Lemma 1 (Monotonicity): The function $V_{fc}(i_{fc})$ given in eq. (1) is monotonically decreasing on the positive real axis (positive cell currents). Specifically, for all $a > 0$ and $b > 0$, it satisfies:

$$(a - b)[V_{fc}(a) - V_{fc}(b)] \leq 0. \tag{2}$$

Proof 1: The proof is established proving that $\frac{dV_{fc}}{di_{fc}} \leq 0$, which is computed as:

$$\frac{dV_{fc}}{di_{fc}} = -a_1 a_2 i_{fc}^{a_2 - 1}, \tag{3}$$

and is clearly non-positive.

Using Kirchhoff's current and voltage laws and a redefinition of variables $x := \text{col}(i_{fc},\ i_{sc},\ v_{sc},\ v_o)$, the average behavior of the system presented in Fig. 1 yields:

$$L_1 \dot{x}_1 = v_{fc} - u_1 x_4 - \nu_1, \tag{4a}$$
$$L_2 \dot{x}_2 = x_3 - u_2 x_4 - \nu_2, \tag{4b}$$
$$C_s \dot{x}_3 = -x_2 - x_3/R_{p3}, \tag{4c}$$
$$C \dot{x}_4 = u_1 x_1 + u_2 x_2 - x_4/R_L, \tag{4d}$$

where $u_1 := 1 - q_1$ is the control signal of the boost converter, the complement of the duty cycle of the switch M_1. The parameters ν_1 and ν_2 comprise the voltage losses caused by parasitic resistances in eqs. (4a) and (4b). Although the largest parasitic resistance originates from the inductor [14], this term also encompasses other parasitic resistances, voltage drops across diodes and switches, and additional unmodeled phenomena. Online estimation of this voltage drop has proven to be effective in the experimental validation of adaptive controllers, as shown in [15]. On the other hand, u_2 is the control signal of the bidirectional converter and is computed according to:

$$u_2 := (1 - q_2)m_1 + q_3(1 - m_1), \tag{5}$$

where $m_1 = \{1,\ 0\}$ is a binary signal that depends on the operation mode. Boost mode with $m_1 = 1$ and buck mode with $m_1 = 0$. Similarly than before, ν_2 comprises the voltage losses caused by parasitic resistances in eq. (4b), primarily the parasitic resistance of the inductor R_{p2}.

Finally, the following assumptions are made to simplify the controller design.

- All state variables i_{fc}, i_{sc}, v_{sc}, v_o, and v_{fc} are assumed to be measurable. Moreover, the parameters L_1, L_2, C_s, and C are considered constant and known, though they may change slowly over time.
- The power switches are assumed ideal. Meaning that switches M_1, M_2, and M_3 have zero on-resistance, and the diodes D and D_p have zero on-resistance and zero voltage drop.
- The voltage losses ν_1 and ν_2 are assumed to converge to constant values during steady-state operation.

III. Controller Design

The control objective of the power system described by eq. (4) is to regulate the SC and output voltages to their respective reference values, $x_3^\star > 0$ and $x_4^\star > 0$, while ensuring a smooth power draw from the cell. As previously discussed, the role of the SC is to handle high and fast transient energy demands, thereby reducing fluctuations in the power extracted from the cell. In steady-state operation, the cell supplies the total power demand, ensuring that the net energy exchange of the SC is zero ($x_2^\star = 0$). The controller design is simplified using singular perturbation theory [16], following a time-scale separation methodology. Accordingly, the system dynamics described by eq. (4) are partitioned into a fast subsystem for currents and a slow subsystem for voltages. Using a current-mode control approach, the controller is designed with two loops: an inner loop adjusts duty cycles to track current reference trajectories, and an outer loop regulates voltages by generating appropriate current references. Both control loops are designed with PI-PBC. This control strategy is described in detail in [17], [18]. Its core concept involves applying a simple PI action over a passive output of the system. This systematic approach ensures global asymptotic stability by designing control laws that stabilize and regulate dynamical systems. A key advantage of this scheme is that convergence is guaranteed for any positive PI gains, greatly simplifying the otherwise complex task of tuning the control gains [13]. Additionally, an adaptive law based on I&I theory is designed to enhance the robustness of the outer loop controller. The

resulting adaptive multi-loop control scheme is detailed in Fig. 3. This diagram illustrates that the core of the PI-PBC is the passive output. It also depicts the required signal flow for both control loops and how the PI action is implemented.

Before designing both control loops, the assignable equilibria compatible with the control objective are determined. To achieve this, after partitioning the dynamics, both subsystems are expressed in a port-controlled Hamiltonian (PCH) formulation. In the fast current partition, the voltages are assumed constant, while in the slow voltage partition, the currents are considered to track their references. Consequently, if the currents are tracking their references, the control signal are also at its reference or equilibria. To begin with, both partitions are obtained with the Facts 1 and 2.

Fact 1 (Inner loop): The *fast* (current) dynamics of eq. (4) can be represented by the PCH system:

$$\mathcal{Q}_c \dot{z} = [\mathcal{J}_c - \mathcal{R}_c] z + g_c u_c + \mathcal{E}_c, \tag{6}$$

where $\mathcal{Q}_c$ is a positive definite inertia matrix, $\mathcal{J}_c$ is a skew-symmetric interconnection matrix, $\mathcal{R}_c$ is a positive semi-definite symmetric matrix, g_c is a port characteristic matrix, and $\mathcal{E}$ is an external disturbance vector, by defining:

$$\mathcal{Q}_c := \begin{bmatrix} L_1 & 0 \\ 0 & L_2 \end{bmatrix},\ z := \begin{bmatrix} x_1 \\ x_2 \end{bmatrix},\ \mathcal{J}_c := 0,\ \mathcal{R}_c := 0, \tag{7a}$$

$$g_c := -x_4 I_2,\ u_c := \begin{bmatrix} u_1 \\ u_2 \end{bmatrix},\ \mathcal{E}_c := \begin{bmatrix} v_{fc} - \theta_{\nu 1} \\ x_3 - \theta_{\nu 2} \end{bmatrix}. \tag{7b}$$

Subsequently, the control signal u_c is obtained when the fast dynamics are in equilibria. For this, the fast dynamics described by eq. (6) are represented in the affine form $\mathcal{Q}_c \dot{z} = f_c(z) + g_c(z) u_c$ with:

$$f_c(z) := [\mathcal{J}_c - \mathcal{R}_c] z + \mathcal{E}_c, \tag{8}$$

then, at equilibria ($\dot{z} = 0$), the control signal is solved from $f_c(z) + g_c(z) u_c^\star = 0$ and computed with the inverse matrix $g_c^{-1}(z) = -1/x_4 I_2$ as follows:

$$g_c^{-1}(z) g_c(z) u_c^\star = -g_c^{-1}(z) f_c(z), \tag{9}$$

$$u_c^\star = -g_c^{-1}(z)([\mathcal{J}_c - \mathcal{R}_c] z + \mathcal{E}_c), \tag{10}$$

$$= \text{col}\left(\frac{v_{fc} - \theta_{\nu 1}}{x_4},\ \frac{x_3 - \theta_{\nu 2}}{x_4} \right), \tag{11}$$

subsequently, the slow dynamics partition is designed.

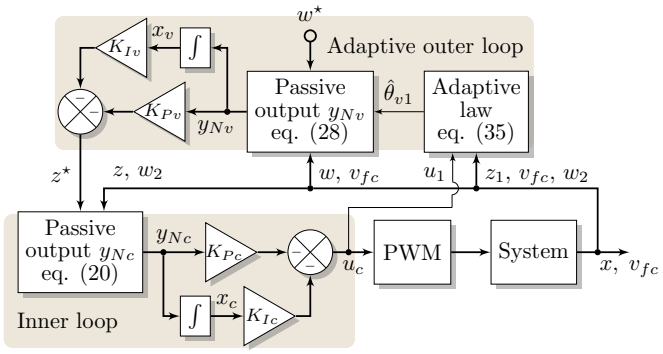

Fig. 3: Schematic diagram of the adaptive multi-loop PI-PBC.

Fact 2 (Outer loop): The *slow* (voltage) dynamics of eq. (4) can be represented by the PCH system:

$$\mathcal{Q}_v \dot{w} = (\mathcal{J}_v - \mathcal{R}_v) w + g_v u_v + \mathcal{E}_v, \tag{12}$$

by defining:

$$\mathcal{Q}_v := \begin{bmatrix} C_s & 0 \\ 0 & C \end{bmatrix},\ w := \begin{bmatrix} x_3 \\ x_4 \end{bmatrix},\ \mathcal{J}_v := 0, \tag{13a}$$

$$\mathcal{R}_v := \begin{bmatrix} \theta_p & 0 \\ 0 & \theta_L \end{bmatrix},\ g_v := \begin{bmatrix} 0 & -1 \\ \frac{v_{fc} - \theta_{\nu 1}}{x_4} & \frac{x_3 - \theta_{\nu 2}}{x_4} \end{bmatrix}, \tag{13b}$$

$$u_v := \begin{bmatrix} z_1^\star \\ z_2^\star \end{bmatrix},\ \mathcal{E}_v := 0, \tag{13c}$$

which is obtained by replacing the control signal of the system of eq. (4) by its equilibria, obtained in eq. (11). Since, in the slow dynamics, the currents are assumed to be at equilibria (track their references). Therefore, the control signals are also at equilibria.

Once both the fast and slow partitions are obtained, the assignable equilibria compatible with the control objective are computed. This is performed in the following lemma.

Lemma 2 (Equilibria): The assignable equilibria of eq. (4) and their corresponding constant inputs are the values contained in the set:

$$\mathcal{E} := \Big\{ (x, u) \in \mathbb{R}^6 :\ x_1 = \frac{\frac{x_3^\star}{R_{p3}}(x_3^\star - \theta_{\nu 2}) + \frac{(x_4^\star)^2}{R_L}}{v_{fc} - \theta_{\nu 1}}, \tag{14a}$$

$$x_2 = -\frac{x_3^\star}{R_{p3}},\ x_3 = x_3^\star,\ x_4 = x_4^\star, \tag{14b}$$

$$u_1 = \frac{v_{fc} - \theta_{\nu 1}}{x_4^\star},\ u_2 = \frac{x_3^\star - \theta_{\nu 2}}{x_4^\star} \Big\}. \tag{14c}$$

Proof 2: Both fast and slow dynamics partitions are used to obtain these values. To begin, the slow dynamics described in eq. (12) are represented in its affine form $\mathcal{Q}_v \dot{w} = f_v(w) + g_v(w) u_v$ where:

$$f_v(w) := [\mathcal{J}_v - \mathcal{R}_v] w + \mathcal{E}_v,$$

this is then evaluated in equilibria, yielding $f_v(w) + g_v(w) u_v^\star = 0$. Subsequently, the reference currents $u_v^\star$ are computed by solving this equation. The inverse matrix $g_v(w)$ is computed as:

$$g_v^{-1}(w) = \begin{bmatrix} (x_3 - \theta_{\nu 2})/(v_{fc} - \theta_{\nu 1}) & x_4/(v_{fc} - \theta_{\nu 1}) \\ -1 & 0 \end{bmatrix}, \tag{15}$$

using this value results in:

$$u_v^\star = -g_v^{-1}(w)([\mathcal{J}_v - \mathcal{R}_v] w + \mathcal{E}_v), \tag{16a}$$

which simplifies to:

$$u_v^\star = \text{col}\left(\frac{\frac{x_3}{R_{p3}}(x_3 - \theta_{\nu 2}) + \frac{x_4^2}{R_L}}{v_{fc} - \theta_{\nu 1}},\ -\frac{x_3}{R_{p3}} \right), \tag{17}$$

that by fixing $x_3 = x_3^\star$ and $x_4 = x_4^\star$ yields the equilibria values of the currents x_1 and x_2 in Lemma 2.

The remaining equilibria are obtained with the fast dynamics of eq. (6). Taking the equilibria values of the control $u_c^\star$ in

eq. (11) and fixing the voltages $x_3 = x_3^\star$ and $x_4 = x_4^\star$ yields the control signals u_1 and u_2 as given in Lemma 2.

Remark 1 (Equilibria): As discussed previously, the control objective is to ensure that, in steady-state operation, the energy supplied or stored by the SC remains at zero. However, in practice, a small leakage current is always present, as shown in eq. (14).

A. Current loop

This control loop leverages the fast dynamics of the system described by eq. (4) to compute the control signals. Its objective is to track the trajectories generated by the outer loop through the duty cycles generation. This inner controller loop can be found in Fig. 3. In the development of the control, the error model (incremental) is used, where the error is defined as:

$$\tilde{x} := x - x^\star, \tag{18}$$

the difference between the state and its reference. Subsequently, using the current dynamics partition of eq. (6), the design of the PI-PBC and its corresponding passive output is outlined in the following proposition.

Proposition 1 (Inner PI-PBC): Consider the closed-loop model of the inner loop eq. (6). Assume that the state z is measurable. Fix a constant current reference as $z^\star \in \mathcal{E}$ and considering the PI-PBC scheme:

$$u = -K_{Pc} y_{Nc} - K_{Ic} x_c + u^\star, \tag{19a}$$
$$\dot{x}_c = y_{Nc}, \tag{19b}$$

where the matrices $K_{Pc} = \text{diag}\{k_{1pc}, k_{2pc}\}$ and $K_{Ic} = \text{diag}\{k_{1ic}, k_{2ic}\}$ are positive definite, and the passive output is defined as:

$$y_{Nc} := \text{col}(-x_4\tilde{z}_1, \ -x_4\tilde{z}_2), \tag{20}$$

then the system converges asymptotically to the equilibria $(z, x_c) = (z^\star, \ 0)$. Where $z^\star \in \mathcal{E}$ denotes the current references and $u^\star \in \mathcal{E}$ is its required duty cycle.

Proof 3: Consider the energy storage function of the storage elements as a candidate Lyapunov function:

$$\mathcal{H}_c(\tilde{z}) = \frac{1}{2}\tilde{z}^\top \mathcal{Q}_c \tilde{z}, \tag{21}$$

which satisfies that $\mathcal{H}_c(0) = 0$ and $\mathcal{H}_c(\tilde{z}) > 0$ whenever $\tilde{z} \neq 0$. Then, by computing its time derivative along the error dynamics of (6):

$$\dot{\mathcal{H}}_c(\tilde{z}) = \tilde{z}^\top \mathcal{Q}_c \dot{\tilde{z}} = \tilde{z}^\top \left(g_c \tilde{u}_c + \begin{bmatrix} v_{fc}(\tilde{z}_1) & 0 \end{bmatrix}^\top\right), \tag{22a}$$
$$= \tilde{z}^\top g_c \tilde{u}_c + (z_1 - z_1^\star)(v_{fc}(z_1) - v_{fc}(z_1^\star)), \tag{22b}$$
$$\leq \tilde{z}^\top g_c \tilde{u}_c = y_{Nc}^\top \tilde{u}_c, \tag{22c}$$

thus, the closed-loop system is passive for the output y_{Nc} of eq. (20). This result is obtained because, in equilibria, the following condition is satisfied:

$$0 = (\mathcal{J}_c - \mathcal{R}_c) z^\star + g_c u_c^\star + \mathcal{E}_c^\star, \tag{23}$$

and in the second line of eq. (30), the monotonicity property of the polarization curve, described in Lemma 1, is employed [13].

For the closed-loop system with the controller, the following candidate Lyapunov function is considered [18]:

$$V_c(\tilde{z}, x_c) = \frac{1}{2}\tilde{z}^\top \mathcal{Q}_c \tilde{z} + \frac{1}{2} x_c^\top K_{Ic} x_c, \tag{24}$$

then, computing its time derivative along the closed-loop system and controller dynamics:

$$\dot{V}(\tilde{z}, \tilde{x}_c) = \tilde{z}^\top \mathcal{Q}_c \dot{\tilde{z}} + x_c^\top K_{Ic} \dot{x}_c, \tag{25a}$$
$$= \tilde{z}^\top g_c \tilde{u} + x_c^\top K_{Ic} y_{Nc}, \tag{25b}$$
$$= -y_{Nc}^\top (K_{Pc} y_{Nc} + K_{Ic} x_c) + x_c^\top K_{Ic} y_{Nc}, \tag{25c}$$
$$= -y_{Nc}^\top K_{Pc} y_{Nc} \leq 0, \tag{25d}$$

hence, by the previous inequality and LaSalle–Yoshizawa's, it is concluded that:

$$\lim_{t\to\infty} z = z^\star. \tag{26}$$

B. Voltage loop

The outer loop leverages the *slow* dynamics of the system described by eq. (4) to generate current references. It aims to achieve voltage regulation by generating current reference trajectories for the inner loop. In Fig. 3 is presented the outer loop controller. This control loop is responsible for the most critical part of the control scheme, generating smooth references for extracting energy from the cell and fast references for managing energy flow to and from the SC. This approach leverages the fast dynamics of the SC to compensate for the slow dynamic response of the cell [19]. On the other hand, it is important to mention that the generation of these trajectories is typically managed by energy management systems, which allocate energy demands among sources while leveraging their specific advantages [20]. Where maximizing fuel (hydrogen) efficiency is a critical objective, particularly in applications such as transportation electrification and microgrids [1]. Finally, using the voltage dynamics partition of eq. (12), the design of the PI-PBC and its corresponding passive output is presented in the following proposition.

Proposition 2: (Outer PI-PBC): Consider the closed-loop of the outer loop described by eq. (12). Assume that the state w is measurable. Fix constant voltage references as $w^\star \in \mathcal{E}$ and consider the PI-PBC scheme

$$u_v = -K_{Pv} y_{Nv} - K_{Iv} x_v + u_v^\star, \tag{27a}$$
$$\dot{x}_v = y_{Nv}, \tag{27b}$$

where the matrices $K_{Pv} = \text{diag}\{k_{1pv}, k_{2pv}\}$ and $K_{Iv} = \text{diag}\{k_{1iv}, k_{2iv}\}$ are positive definite, and the passive output is defined as:

$$y_{Nv} := \text{col}\left(\tilde{w}_2 \frac{v_{fc} - \theta_{\nu 1}}{w_2}, \ \ \tilde{w}_2 \frac{w_1 - \theta_{\nu 2}}{w_2} - \tilde{w}_1\right), \tag{28}$$

then, the system converges asymptotically to the equilibria $(w, x_v) = (w^\star, \ 0)$. Where $w^\star \in \mathcal{E}$ denotes the fixed voltage references and $u_v^\star \in \mathcal{E}$ represents its required current references.

Proof 4: Consider the energy storage elements of eq. (12) to design the following candidate Lyapunov function:

$$\mathcal{H}_v(\tilde{w}) = \frac{1}{2}\tilde{w}^\top \mathcal{Q}_v \tilde{w}, \tag{29}$$

that satisfies $\mathcal{H}_v(0) = 0$ and $\mathcal{H}_v(\tilde{w}) > 0$ whenever $\tilde{w} \neq 0$. Then, by computing its time derivative along the error dynamics of eq. (12):

$$\dot{\mathcal{H}}_v(\tilde{w}) = \tilde{w}^\top \mathcal{Q}_v \dot{\tilde{w}} = \tilde{w}^\top \big(-\mathcal{R}_v \tilde{w} + g_v \tilde{u}_v \big), \tag{30a}$$

$$\leq \tilde{w}^\top g_v \tilde{u}_v = y_{Nv}^\top \tilde{u}_v, \tag{30b}$$

thus, the closed-loop system is passive for the output y_{Nv} of eq. (28). Similarly to before, this result is obtained by leveraging the fact that, at equilibria, the following condition is satisfied:

$$0 = (\mathcal{J}_v - \mathcal{R}_v) w^\star + g_v u_v^\star + \mathcal{E}_v^\star. \tag{31}$$

For the closed-loop system with the controller, the following candidate Lyapunov function is considered:

$$V_v(\tilde{w}, x_v) = \frac{1}{2} \tilde{w}^\top \mathcal{Q}_v \tilde{w} + \frac{1}{2} x_v^\top K_{Iv} x_v, \tag{32}$$

then, computing its time derivative along the closed-loop system and controller dynamics:

$$\dot{V}(\tilde{w}, \tilde{x}_v) = \tilde{w}^\top \mathcal{Q}_v \dot{\tilde{w}} + x_v^\top K_{Iv} \dot{x}_v, \tag{33a}$$

$$= -\tilde{w}^\top \mathcal{R}_v \tilde{w} + \tilde{w}^\top g_v \tilde{u}_v + x_v^\top K_{Iv} y_{Nv}, \tag{33b}$$

$$= -\tilde{w}^\top \mathcal{R}_v \tilde{w} - y_{Nv}^\top (K_{Pv} y_{Nv} + K_{Iv} x_v) + \tag{33c}$$

$$x_v^\top K_{Iv} y_{Nv}, \tag{33d}$$

$$= -\tilde{w}^\top \mathcal{R}_v \tilde{w} - y_{Nv}^\top K_{Pv} y_{Nv}, \tag{33e}$$

$$\leq -\tilde{w}^\top \mathcal{R}_v \tilde{w}, \tag{33f}$$

thus, by applying the previous inequality and LaSalle–Yoshizawa's theorem, it is concluded that:

$$\lim_{t \to \infty} w = w^\star. \tag{34}$$

C. Adaptive law

As observed in the controller design, the passive output y_{Nv} in Proposition 2 depends on the voltage loss uncertainties ν_1 and ν_2. To address this, an adaptive law based on I&I theory is designed, enhancing the robustness of the outer loop controller. The objective is to compute an estimate $\hat{\theta}_{\nu 1}$ of the voltage loss $\theta_{\nu 1}$ and incorporate it in a *certainty-equivalent* way into the outer loop PI-PBC. It is worth mentioning that the application of I&I theory has been widely reported in the design of parameter estimators, stabilizing control laws, and state observers for nonlinear systems. According to [21], this estimation is obtained using two terms, one integral and one proportional. The proposed online estimator is designed with the following proposition.

Proposition 3 (Parameter estimator): The I&I estimator designed as:

$$\dot{\xi} = \alpha x_1^2 \Big(v_{fc} - u_1 x_4 - \xi + \frac{\alpha_1}{3} L_1 x_1^3 \Big), \tag{35a}$$

$$\hat{\theta}_{\nu 1} = \xi - \frac{\alpha}{3} L_1 x_1^3, \tag{35b}$$

where α is a positive gain and $x_1 \notin \mathcal{L}_2$, satisfies that the estimation error $\tilde{\theta}_{\nu 1}$:

$$\lim_{t \to \infty} |\tilde{\theta}_{\nu 1}| = 0, \tag{36}$$

with all signals remaining bounded.

Proof 5: Taking the time derivative of the estimation error $\tilde{\theta}_{\nu 1}$ yields:

$$\dot{\tilde{\theta}}_{\nu 1} = \dot{\hat{\theta}}_{\nu 1} - \dot{\theta}_{\nu 1}, \tag{37a}$$

$$= \dot{\xi} - \alpha L_1 x_1^2 \dot{x}_1, \tag{37b}$$

$$= \alpha x_1^2 \Big(v_{fc} - u_1 x_4 - \xi + \frac{\alpha_1}{3} L_1 x_1^3 - L_1 \dot{x}_1 \Big), \tag{37c}$$

$$= \alpha x_1^2 \Big(v_{fc} - u_1 x_4 - \hat{\theta}_{\nu 1} - [v_{fc} - u_1 x_4 - \theta_{\nu 1}] \Big), \tag{37d}$$

$$= -\alpha x_1^2 \tilde{\theta}_{\nu 1}, \tag{37e}$$

where the second line is obtained by assuming that the uncertainty varies slowly compared to the dynamics of the estimator; hence, $\dot{\theta}_{\nu 1} = 0$. And the fourth line through the relation eq. (35b). Then, computing the solution of eq. (37e) yields:

$$\tilde{\theta}_{\nu 1}(t) = \tilde{\theta}_{\nu 1}(0) e^{-\alpha \int x_1^2 dt}, \tag{38}$$

hence, it follows that $\tilde{\theta}_{\nu 1} \to 0$ iff $x_1 \notin \mathcal{L}_2$.

The resulting adaptive control scheme is presented in Fig. 3. As observed, the main challenge of this control approach lies in obtaining both passive outputs. Both control loops are inherently robust, as they do not require knowledge of the load, which is an uncertain and time-varying parameter in practice. This robustness ensures that the stability of the control strategy is maintained without relying on load information. Making it feasible to be extended for higher power levels, like an isolated DC microgrid. However, to support distributed generation and fault tolerance, some aspects need to be improved, as detailed in [9]. Additionally, if the goal is to supply AC voltage, the system must address the synchronization issue with other systems in the grid.

Remark 2: Designing an adaptive law to estimate the voltage loss ν_2 presents challenges due to the lack of persistent excitation in steady-state conditions. Because the control objective is to have zero energy supplied or stored by the SC in steady-state, leading to short variation in its current. Thus, the condition required for the estimation to converge, $x_2 \notin \mathcal{L}_2$, is not met. This results in insufficient excitation for its estimation, causing the estimation error to remain bounded but not converge to zero. Moreover, it is assumed that the integral action of the controller can handle effectively this uncertainty.

Remark 3: It is important to note that the design of this adaptive controller assumes the availability of full state measurements in addition to cell voltage. However, in real-world environments, this may not always be feasible, necessitating the design of observers. Although this aspect lies beyond the scope of this paper, it remains a crucial consideration.

IV. Numerical results

Numerical simulations validate the correct performance of the controller by regulating both the output voltage and SC voltage to some references $x_3^\star$ and $x_4^\star$, while ensuring smooth variation of the PEMFC current, using Simulink/MATLAB. To enhance the realism of the system, the simulation incorporates the power function model of the 1.2 kW Nexa® as the PEMFC

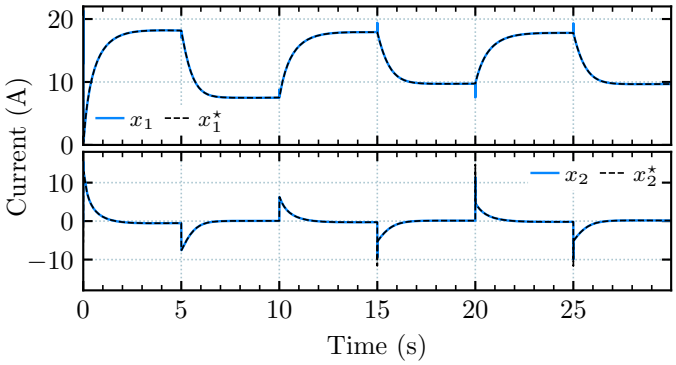

Fig. 4: Numerical simulation results: The cell current and SC current are shown alongside their respective references, showing that fast transients are managed by the SC, while the cell handles the steady-state energy demand.

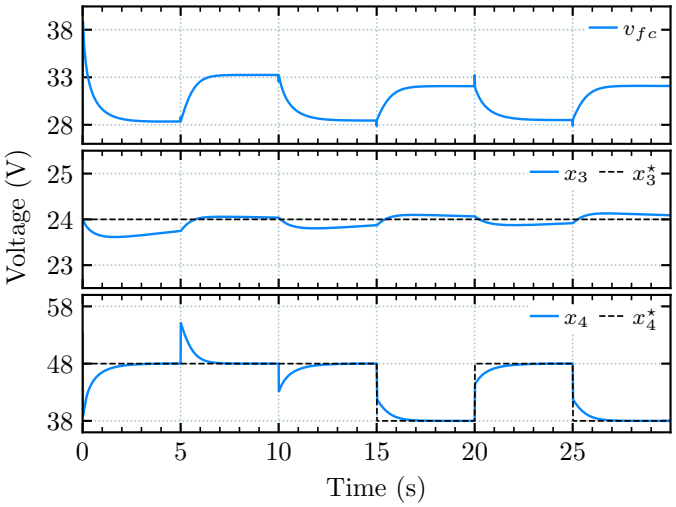

Fig. 5: Numerical simulation results: The SC voltage and output voltage are regulated to their respective references, meanwhile the cell voltage has smooth variations.

source. Experimental measurements from this module are utilized to obtain the open-circuit voltage (E_{oc}) under no-load conditions. These measurements are displayed in Fig. 2. Then, with the average values, offline data-fitting procedures are performed to determine the values of parameters a_1 and a_2 in eq. (1). It is important to mention that this model captures the average behavior and does not account for the complex hysteresis phenomena, which is a characteristic of the cell dynamics, as can be seen in Fig. 2. The simulation is carried out using the system parameters and control gains reported in Table I. As outlined before, the integration of a SC into the fuel cell system through a bidirectional converter aims to manage fast and high transients. Therefore, the rapid dynamics of the SC are leveraged to compensate for the slow dynamic response of the fuel cell, enhancing the system performance and longevity. This makes it particularly attractive for applications in DC microgrids and transportation electrification. Regarding the control gains, unfortunately, there is no optimized method to tune them. These gains are empirically adjusted. In the inner loop, both current references are tracked using identical proportional and integral gains. Starting with small values, they were gradually increased until the tracking error between the measured currents and their references became negligible under pulsating conditions. For the adaptive law, the gain is gradually increased from an initial value of 0.1 until, even under pulsating conditions, the difference between the actual signal and its estimated value is indistinguishable. Finally, when tuning the outer loop gains, it is taken into account that the proportional gain primarily influences the response speed, while the integral gain determines the overall response time. Thus, the proportional gains are adjusted to assign a higher value to the SC, while the integral gains are adjusted to assign a higher value to the cell. These gains are tuned until the desired response is obtained. Supply transient power by the SC and steady-state power by the cell. Allowing the SC to respond quickly to fluctuations in demand while the cell supplies the steady-state demand.

Numerical results of the system dynamics response are presented in Figs. 4 to 7. Throughout the test, the SC voltage reference is fixed at $x_3^\star$ =24.0 V. Then, the output voltage reference is set to $x_4^\star = 48.0\,\text{V}$ (500 W), with the load pulsating between $9.216\,\Omega$ (250 W) and $4.608\,\Omega$ (500 W) at 0.1 Hz. After 15 seconds, the load is fixed at $4.608\,\Omega$, and the output voltage reference pulsates between $x_4^\star = 48.0\,\text{V}$ (500 W) and $x_4^\star = 38.0\,\text{V}$ (314 W) at the same frequency of 0.1 Hz. As shown in Fig. 4, it is evident that the current references are accurately tracked despite pulsating changes in load or output voltage reference. This indicates that the inner loop is effectively adjusting the control signals within achievable ranges, as can be seen in Fig. 7. Additionally, as desired, the cell current exhibits smooth variations, even under pulsating changes in load or reference voltage, maintaining values between about 5.50 A and 20.0 A. Thus, the SC is supplying or storing energy during fast transients, before gradually reaching zero. This current takes values around -14.0 A and 14.0 A. As observed in Fig. 6, the voltage loss is accurately estimated, with the difference between the actual value and the estimate being negligible, except during some pulsating changes. And finally, as previously mentioned, the control objective is the regulation of both the output voltage and the SC voltage. As shown in Fig. 5, the outer loop achieves this by generating appropriate reference currents to regulate them. The regulation of both the SC voltage and the output voltage to their respective references confirms the proper functioning of the outer control loop. Additionally, the voltage supplied by the cell exhibits smooth variations, ranging from 27.0 V to 34.0 V. Throughout the simulation, the SC voltage is effectively regulated at 24.0 V, with minimal variations of less than 1.0 V. This result highlights the nature of the SC, as it can handle high charge and discharge currents without a degradation of its lifespan. The output voltage is tightly regulated despite pulsating changes in load or voltage reference, maintaining values between 37.5 V and 58.0 V.

V. Concluding Remarks

In this paper, a PI-PBC approach for a system consisting of a PEMFC as the primary energy source and a SC as an

TABLE I: System parameters and control gains

Parameters	Values	Parameters	Values	Gains	Values
L_1	38.63 μH	E_{oc}	40.45 V	K_{Ic}	$10.0I_3$
L_2	44.69 μH	a_1	2.219	K_{Pc}	$5.0\times10^{-5}I_3$
C_s	12.5 F	a_2	0.5848	K_{Iv}	diag$\{12,\ 0.5\}$
C	263.4 μF	R_{p3}	1.00 MΩ	K_{Pv}	diag$\{21\times10^{-5}, 2.1\}$
R_{p1}	8.30 mΩ	R_L	4.608 Ω	α	1.0
R_{p2}	10.5 mΩ				

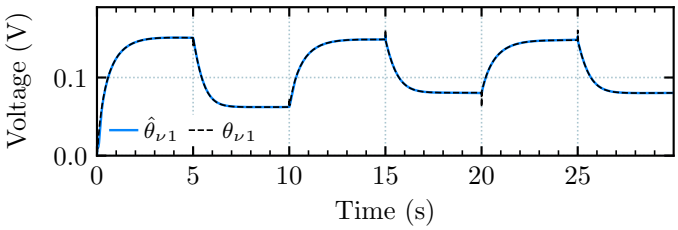

Fig. 6: Numerical simulation results: Online estimation through I&I of the voltage loss $\hat{\theta}_{\nu 1}$.

auxiliary storage device was presented. The control objective was to regulate the output and SC voltages while ensuring smooth variations in the energy extracted from the cell, even under fluctuating energy demand. The controller design is simplified by invoking the singular perturbation theory. Hence, by the difference in time scales, the system dynamics can be partitioned in *fast for currents* and *slow for voltages*. Then, the controller is designed with current-mode control. Both control loops were developed using the PI-PBC methodology. An inner loop adjusts the duty cycles for tracking current reference trajectories, while an outer loop generates these current references to regulate the voltages. Additionally, an adaptive law based on I&I theory is designed to enhance the robustness of the outer loop controller. Numerical results demonstrate the effective performance of the closed-loop system, maintaining stability and proper regulation despite pulsating variations in energy demand. Finally, future work is towards a connection of the fuel cell system with a SC-based energy storage system to support the grid under grid-following and grid-forming modes, and consider issues such as synchronization, harmonic mitigation, voltage regulation and dynamic interaction with other grid-connected systems.

References

[1] K. Jiao, J. Xuan, Q. Du, Z. Bao, B. Xie, B. Wang, Y. Zhao, L. Fan, H. Wang, Z. Hou, S. Huo, N. P. Brandon, Y. Yin, and M. D. Guiver, "Designing the next generation of proton-exchange membrane fuel cells," *Nature*, vol. 595, pp. 361–369, 7 2021.

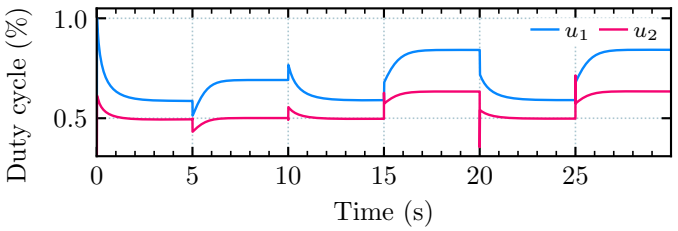

Fig. 7: Numerical simulation results: Control signals adjusting to track its current reference while taking achievable values.

[2] Y. Wang, B. Seo, B. Wang, N. Zamel, K. Jiao, and X. C. Adroher, "Fundamentals, materials, and machine learning of polymer electrolyte membrane fuel cell technology," *Energy and AI*, vol. 1, p. 100014, 8 2020.

[3] A. Benmouna, M. Becherif, D. Depernet, C. Dépature, and L. Boulon, "Nonlinear control and optimization of hybrid electrical vehicle under sources limitation constraints," *International Journal of Hydrogen Energy*, vol. 45, pp. 11 255–11 266, 4 2020.

[4] A. Tofighi and M. Kalantar, "Passivity-based control of pem fuel cell/battery hybrid power source," in *2011 IEEE Energy Conversion Congress and Exposition*. IEEE, 9 2011, pp. 902–908.

[5] ——, "Adaptive passivity-based control of pem fuel cell/battery hybrid power source," *Przegląd Elektrotechniczny*, vol. 87, no. 4, pp. 164–171, 2011.

[6] Y. A. Zuniga-Ventura, D. Langarica-Cordoba, J. Leyva-Ramos, L. H. Diaz-Saldierna, and V. M. Ramirez-Rivera, "Adaptive backstepping control for a fuel cell/boost converter system," *IEEE Journal of Emerging and Selected Topics in Power Electronics*, vol. 6, pp. 686–695, 6 2018.

[7] L. Hao and Y. Fan, "Modeling and passivity-pi control of a fuel cell-supercapacitor hybrid energy storage system," in *2018 IEEE International Conference on Mechatronics, Robotics and Automation (ICMRA)*. IEEE, 5 2018, pp. 17–21.

[8] A. Benmouna, M. Becherif, J. Chen, H. Chen, and D. Depernet, "Interconnection and damping assignment passivity based control for fuel cell and battery vehicle: Simulation and experimentation," *International Journal of Hydrogen Energy*, vol. 44, pp. 22 467–22 477, 8 2019.

[9] L. Martínez, D. Fernández, and R. Mantz, "Passivity-based control for an isolated dc microgrid with hydrogen energy storage system," *International Journal of Hydrogen Energy*, vol. 67, pp. 1262–1269, 5 2024.

[10] Y. A. Zuniga-Ventura, J. Leyva-Ramos, L. H. Diaz-Saldiema, I. A. Diaz-Diaz, and D. Langarica-Cordoba, "Nonlinear voltage regulation strategy for a fuel cell/supercapacitor power source system," in *IECON 2018 - 44th Annual Conference of the IEEE Industrial Electronics Society*. IEEE, 10 2018, pp. 2373–2378.

[11] L. Diaz-Saldierna, J. Leyva-Ramos, D. Langarica-Cordoba, and M. Ortiz-Lopez, "Energy processing from fuel-cell systems using a high-gain power dc-dc converter: Analysis, design, and implementation," *International Journal of Hydrogen Energy*, vol. 46, pp. 25 264–25 276, 7 2021.

[12] L. Zhang, X. Hu, Z. Wang, F. Sun, and D. G. Dorrell, "A review of supercapacitor modeling, estimation, and applications: A control/management perspective," *Renewable and Sustainable Energy Reviews*, vol. 81, pp. 1868–1878, 1 2018.

[13] R. Cisneros, R. Ortega, C. A. Beltrán, D. Langarica-Cordoba, and L. H. Díaz-Saldierna, "Output voltage regulation of a fuel cell/boost converter system with uncertain load: An adaptive pi-pbc approach," *International Journal of Adaptive Control and Signal Processing*, vol. 37, pp. 2349–2363, 9 2023.

[14] D. Langarica-Cordoba, P. R. Martinez-Rodriguez, L. H. Diaz-Saldierna, J. Leyva-Ramos, D. Reyes-Cruz, and S. Iturriaga-Medina, "Passivity-based control for a dc/dc high-gain transformerless boost converter," *Asian Journal of Control*, vol. 25, pp. 26–39, 1 2023.

[15] D. Reyes-Cruz, P. Martinez-Rodriguez, D. Langarica-Cordoba, G. Vazquez-Guzman, J. Sosa-Zuñiga, and V. Ramirez-Rivera, "Control strategies and experimental validation for high-gain non-isolated double inductor boost converter," *Engineering Science and Technology, an International Journal*, vol. 37, p. 101294, 1 2023.

[16] H. Khalil, *Nonlinear Systems*, 3rd ed. Prentice Hall, 2001.

[17] R. Ortega, J. G. Romero, P. Borja, and A. Donaire, *PID Passivity-Based Control of Nonlinear Systems with Applications*. IEEE Press-Wiley, 2021.

[18] M. Hernandez-Gomez, R. Ortega, F. Lamnabhi-Lagarrigue, and G. Escobar, "Adaptive pi stabilization of switched power converters," *IEEE Transactions on Control Systems Technology*, vol. 18, no. 3, pp. 688–698, 2009.

[19] A. Noori, M. F. El-Kady, M. S. Rahmanifar, R. B. Kaner, and M. F. Mousavi, "Towards establishing standard performance metrics for batteries, supercapacitors and beyond," *Chemical Society Reviews*, vol. 48, pp. 1272–1341, 3 2019.

[20] Y. Zhou, H. Obeid, S. Laghrouche, M. Hilairet, and A. Djerdir, "A novel second-order sliding mode control of hybrid fuel cell/super capacitors power system considering the degradation of the fuel cell," *Energy Conversion and Management*, vol. 229, p. 113766, 2 2021.

[21] A. Astolfi, D. Karagiannis, and R. Ortega, *Nonlinear and Adaptive Control with Applications*. Springer London, 2008.